Available online at www.sciencedirect.com
ScienceDirect
Polymer 47 (2006) 6311–6321
polymer
www.elsevier.com/locate/polymer

Time-resolved light scattering of the phase separation in polymer-dispersed liquid crystals formed by photo-polymerization induced phase separation

N.J. Crawford [a], M.D. Dadmun [a,*], T.J. Bunning [b], L.V. Natarajan [b]

[a] *Department of Chemistry, University of Tennessee, Buehler Hall, Knoxville, TN 37996-1600, USA*
[b] *Materials Research Directorate, Air Force Research Laboratories, Wright-Patterson Air Force Base, USA*

Received 5 May 2006; received in revised form 23 June 2006; accepted 26 June 2006
Available online 1 August 2006

Abstract

Time-resolved light scattering is utilized to monitor the phase separation of photo-initiated polymer-dispersed liquid crystals. At the lowest cure intensities studied, the system undergoes spinodal decomposition and the results are analyzed with Cahn–Hilliard theory. As the cure intensity increases, the rate of phase separation increases such that the early stages of spinodal decomposition are no longer observable. These systems are analyzed using the Debye–Bueche model, which provides the time evolution of the number and size of LC domains. These results indicate that an increase in cure beam intensity initially increases the rate of domain growth, but this effect is overwhelmed by the fast vitrification and cross-linking that can occur at highest cure beam intensities.

Keywords: Time-resolved light scattering; Polymer-dispersed liquid crystals; Phase separation

1. Introduction

Polymer-dispersed liquid crystals, or PDLCs, have been the subject of considerable interest in the construction of new electro-optical devices. These composite materials consist of droplets of liquid crystals (LCs) distributed throughout a polymer matrix [1–7]. The anisotropic LCs can change from opaque to transparent with the application of an electric field while the matrix provides mechanical strength as well as the ability to control the configuration of the LC droplets. Such properties have allowed PDLCs to be used in the construction of holographic diffraction gratings, reflection gratings, privacy windows, and even show promise as materials for switchable photonic crystals [6]. A vitally important method used to construct PDLC devices is photo-polymerization induced phase separation, or PIPS. The process starts with a homogeneous mixture of LC, multi-functional monomer, and photo-initiator. When polymerization begins, usually by a free radical reaction, the rapid formation of a cross-linked polymer matrix thrusts the blend into thermodynamic instability, similar to a continuous thermal quench [7]. As the polymerization continues, the cross-linking of the polymer matrix stops the phase separation of LC upon the complete gelation and subsequent vitrification of the matrix [18].

In order to optimize the electro-optical performance of PDLC devices, factors that affect the final morphology of PDLCs that are produced by PIPS must be understood. Some of these factors include LC solubility, LC content, monomer functionality, as well as the polymerization rate. LC solubility [1–4] in the resulting polymer matrix determines the percentage of LC that is able to remain phase separated and, as a result, has been the subject of many studies [3,5,8–15]. The LC content plays a vital role in PIPS by affecting not only the size of the domains but also the trajectory of the blend as it is moved through phase space on polymerization. This factor has also been the subject of works by Serbutoviez et al. and more recently by Vaia and co-workers [16–18]. The choice of monomer, especially if it is multi-functional,

* Corresponding author. Tel.: +1 865 974 6582.
E-mail address: dad@utk.edu (M.D. Dadmun).

0032-3861/$ - see front matter © 2006 Elsevier Ltd. All rights reserved.
doi:10.1016/j.polymer.2006.06.058

can drastically change the cross-link density within the PDLC, a condition that has been shown by Pogue et al. [19] to alter the size, shape, and the number of LC domains. Factors that affect the polymerization rate, such as temperature, reaction chemistry, or, in the case of photo-polymerization, illumination intensity, are also vitally important because of their obvious effect on the formation of the polymer matrix itself. Studies have been carried out to determine the impact of changing the temperature and reaction chemistry on the resultant PDLC morphology. Additionally, the effect of the cure intensity on phase separation kinetics has been examined on UV-cured systems [20].

The trajectory of the sample through phase space as it undergoes phase separation in PIPS is complex, as the system may be thrust from the metastable to the unstable regions as the polymerization proceeds. As the system enters the metastable region, newer domains may form between the existing domains due to heterogeneous nucleation, thus the inter-domain distance could become smaller with the progression of the polymerization process. There may be a cross-over from nucleation to spinodal decomposition, as the coexistence line passes through the metastable region before reaching the unstable region as the polymerization proceeds [21]. A further complexity arises from the fact that the supercooling (the temperature difference between the coexistence line and the reaction temperature) increases as the polymerization proceeds, which in turn can make the domains smaller. This process may compete with the intermediate stage of spinodal decomposition which grows the domain size to create a Cahn–Hilliard linear region that is longer than expected [22].

In order to probe the complex phase separation process that occurs during PIPS, different experimental techniques have been employed. Optical microscopy (OM) has been a commonly used technique to observe the formation of LC domains [4,5]. Complimentary to OM, differential scanning calorimetry is employed to monitor the polymerization reaction as well as the emergence of the LC domains, signified by the appearance of liquid crystalline transitions [5]. Scanning electron microscopy, or SEM, is employed in several studies to examine the morphology of the polymer matrix but only after the LC is removed [18,19]. Scattering techniques, specifically light and X-ray, are used to observe morphological changes over the sample volume. Time-resolved light scattering (TRLS), in particular, offers a non-destructive method to continuously monitor phase separation on length scales of hundreds of nanometers to microns. However, the experiments that exploit this technique have been very limited in number [20].

The purpose of this work is to utilize TRLS to study the phase separation kinetics of PDLC syrups used for holographic gratings. The impact of two of the factors mentioned previously, LC content and cure intensity, on the phase separation process is examined. The syrups used in this study contain 40% and 50% by weight of the LC E7, compositions that have been shown by Vaia et al. [18] to yield different matrix morphologies. The role of light intensity on PIPS is determined by examining the curing of both LC compositions at four different intensities; 0.069, 0.14, 0.21, and 0.69 mW/cm^2. This range of light intensities should provide a range of rates of matrix formation which, in turn, should yield varying phase separation behavior.

2. Experimental

2.1. Materials and sample preparation

The syrups used in this study consist of the liquid crystal E7, dipentaerythritol dipentaacrylate monomer, *N*-phenyl glycine and Rose Bengal for photo-initiation, and *N*-vinyl pyrrolidone as a homogenizing agent. Samples from the syrups are prepared under dark room conditions by pipetting onto quartz windows. Each window has a 0.01 mm deep cup to ensure the sample is uniform in thickness.

2.2. Time-resolved light scattering

Time-resolved light scattering experiments are performed at ambient temperature (25 °C) using an instrument based on the one employed by Sato and Han [23]. The probe beam originates from a 20 mW He–Ne laser that passes through a pinhole to a lens that focuses the beam on the sample, held perpendicular to the beam. Scattered light from the sample is collected by collimation lenses, passed through a red Kodak filter to remove stray green light, and focused onto a 512 pixel photodiode array detector (Princeton Instruments, RY-512). Control of the angle for the collimation lenses and detector is provided by a goniometer. Data from the detector are collected by a controller (Princeton Instruments, ST-120) connected to a PC. Control of exposure times for the scattering experiments as well as the number of spectra recorded is accomplished by the PC running WinSpec v. 1.0. Scattering data for all the experiments are collected continuously every 0.1 s over 400 s periods throughout the course of each experiment. The data are plotted as intensity versus the wave vector, q, where

$$q = (4\pi/\lambda)\sin(\theta/2) \quad (1)$$

Here λ is the wavelength of the incident radiation, the He–Ne beam, and θ is the angle corresponding to each pixel.

The cure beam is produced by a 3 mW green diode laser (532 nm, B & W Tek, Inc.) passed through a narrow band pass interference filter (532 nm, Edmund Industrial Optics). In order to ensure the uniform illumination of the sample we employ two different optical elements, a diffusion plate placed between the beam emerging from the band pass filter and the sample or a double concave lens (focal length −30 mm) located between the diode laser and the band pass filter. Due to the attenuation of the cure beam by the diffusion plate, it is only used for the lowest cure intensity, 0.069 mW/cm^2, while for the higher cure beam intensities, 0.14–0.69 mW/cm^2, the cure beam is defocused to give complete sample illumination. The intensity of the cure beam at the sample is controlled by adjusting the distance of the diode laser to the lens. Cure beam intensities are measured with a digital light meter (Lutron LX-101A) held at the sample holder.

2.3. HRSEM

Samples for high resolution scanning electron microscopy, or HRSEM, are prepared by removing the E7 by soaking the fully cured films in methanol overnight. The films are dried in vaccuo for HRSEM. The images are analyzed by Image J, the java-based version of NIH Image.

3. Results and discussion

3.1. Samples illuminated with 0.069 mW/cm^2

Representative light scattering profiles for the phase separation process of both 40% and 50% E7 samples illuminated at 0.069 mW/Cm^2 are given in Fig. 1a–d. The plots consist of smoothed data obtained by subtracting the background from each spectrum. The profiles are plotted as intensity, in arbitrary units, versus wave vector, q, in μm^{-1}.

Fig. 1a and b shows data for the 40% E7 sample for experiment times of 30–3245 s. The early stages of the experiment do not exhibit any change from the background until 221 s when scattering profiles show the appearance of a distinct maximum at $q \sim 4.7\ \mu m^{-1}$. This delay in structural growth may be related to the presence of an induced stage in the radical polymerization process, where inhibitors that are naturally present in the sample, such as oxygen, are consumed. The maximum grows steadily in intensity at the same wave vector until the time reaches 1020 s. The peak undergoes a shift to a lower q at 1120 s and continues to grow with time. During the later stages of the experiment, we observe the formation of multiple peaks for times greater than 1325 s. The complex scattering profiles for these later times make the determination of a single maximum difficult. When the experiment reaches ~3000 s, the growth of the scattering intensity slows until there is a little change between the profile observed at 3195 s and 3245 s.

The scattering data that are given in Fig. 1c and d show the scattering data for the 50% E7 sample. No difference between the background and the measured intensity is observed for very early stages of the experiment. Around 107 s the scattering

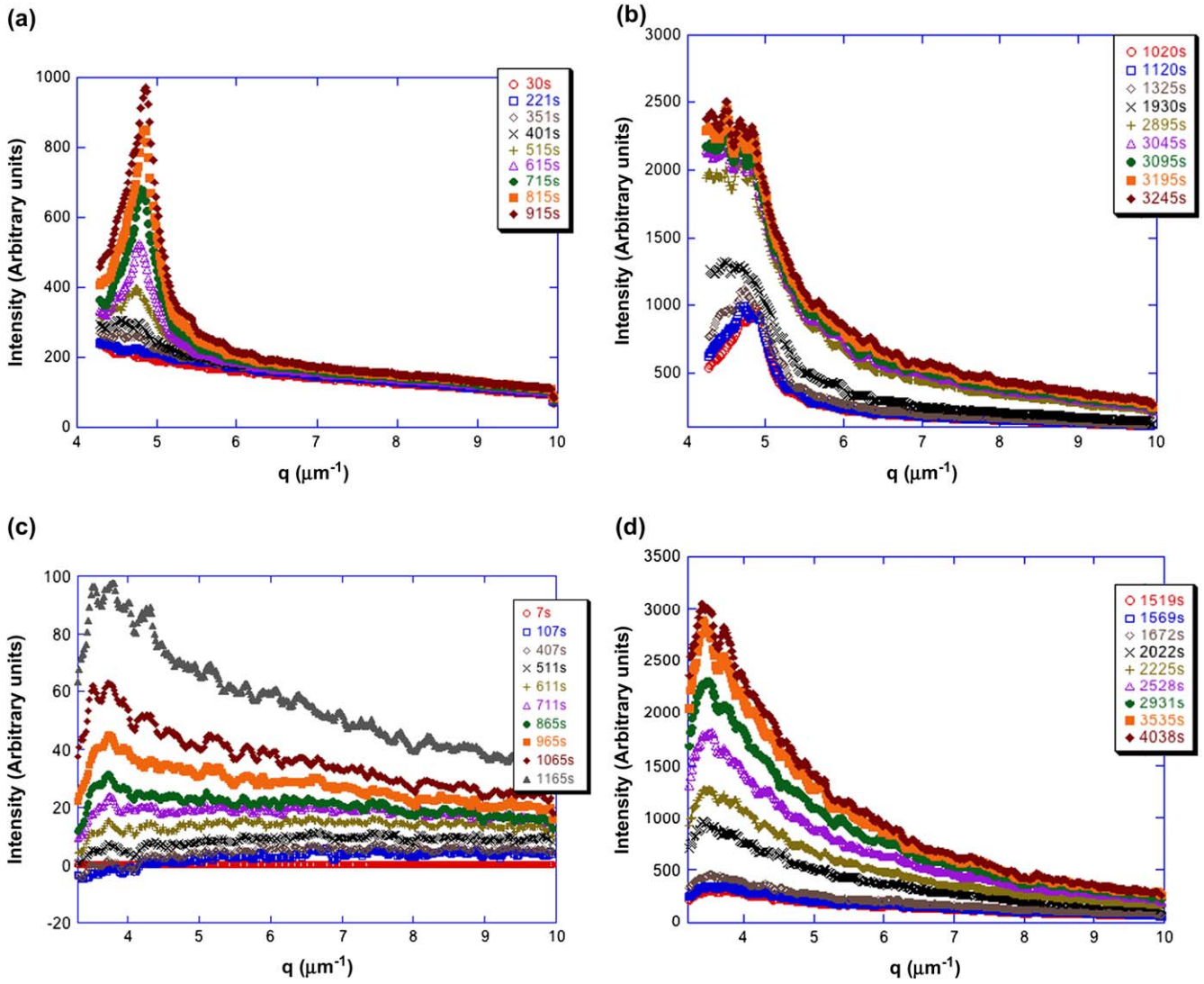

Fig. 1. Scattering profiles for blends cured at 0.069 mW/cm^2. (a) 40% E7 30–915 s; (b) 40% E7 1020–3245 s; (c) 50% E7 7–1165 s; (d) 50% E7 1519–4038 s.

becomes very broad and increases slowly in intensity through 511 s. The maximum that appears during this stage is more difficult to discern than in the 40% E7 samples, however, we estimate the value to fall between $q \sim 6.8$ and $q \sim 6.4\ \mu m^{-1}$. The maximum in the scattering shows a shift to lower q-values, from 5.6 to 3.7 μm^{-1}, as the time progresses from 611 s to 711 s. Throughout the remainder of the experiment, 865–1165 s in Fig. 1c and all times in Fig. 1d, the profile is dominated by a single maximum that remains between 3.7 and 3.4 μm^{-1}. The peak intensity continues to grow with time until 4038 s when there is no further change in the scattering.

From the scattering data in Fig. 1 we observe features that are shared by both LC compositions studied at this cure intensity and reveal more details regarding the phase separation mechanism. One common feature to both compositions is the delay in time between the start of the experiment and the appearance of a maximum in the scattering. This gap, called the induction period [24–28], corresponds to the delay in phase separation from the growth of the polymer matrix. In other words, for the system to favor phase separation of the blend into LC-rich and gel-rich domains, the polymerization must generate matrix material of sufficiently large molecular weight to induce thermodynamic instability. The second feature common to both blends has to do with the appearance of a single maximum in the scattering that not only grows in intensity but also changes in scattering vector with time. Similar behavior has been observed experimentally by Nwabunma et al. [27] as well as in the numerical results of Maugey and co-workers [29] as strong support for phase separation by spinodal decomposition, or SD [30–34]. Lastly, when the scattering profiles no longer change, the phase separation process has been effectively arrested, an event that is attributed by Pogue et al. [19] to the vitrification of the polymer matrix.

The presence of the scattering maxima in both experiments corresponds to the formation of LC-rich and polymer-rich domains that possess an average spacing, or inter-domain distance, Λ [30]. The scattering vector for the maximum, q_m, is related to Λ by Eq. (2). Fig. 2 is a plot of Λ as a function of illumination time for both compositions. For the 40% E7 syrup, Λ shows only small changes with illumination time,

$$q_m = 2\pi/\Lambda \tag{2}$$

from 1.32 to 1.33 μm, during the course of phase separation. In contrast, the 50% E7 sample begins with much smaller inter-domain distances, around 0.9 μm, but undergoes a definite increase after 511 s until, for the final stages of the experiment, Λ levels off to a value that is twice as large, ~1.8 μm.

The difference in the inter-domain distance for the two LC compositions highlights the effect of increasing LC content on the phase separation process. In terms of the time needed for Λ to reach an average value, the 40% E7 sample reaches this point roughly three times faster than the 50% E7 system. The 50% E7 sample also exhibits Λs that are twice as large as the 40% samples. Both of these observations are consistent with previous results by Vaia et al. [18] who explained this result in terms of how the LC content changes the PIPS process.

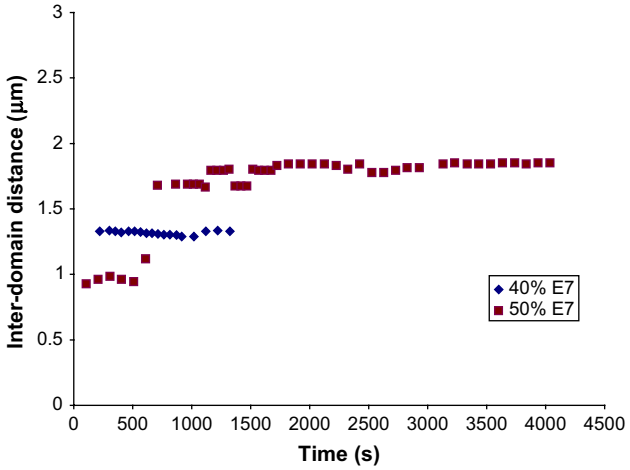

Fig. 2. Plot of inter-domain distance versus time for both LC compositions 40% E7 (◆) and 50% E7 (■).

First, when the LC content is increased, the monomer concentration decreased, a condition that slows the formation of the polymer matrix, thus the 40% sample reaches the equilibrium Λ for the system much faster than the 50% sample. The greater LC content also changes the mass transport within the system by increasing the mobility of the matrix material and LC. Thus, the 50% sample has more mobility during the phase separation process, as well as slower matrix formation (as evidenced by slower phase separation), a combination of conditions that results in larger inter-domain distances at long illumination times.

During the early stages of SD [30–33], composition fluctuations exhibit a dominant length scale that results in a maximum in the scattering profile, and the morphology of the phase-separating components is characterized by an interconnected structure. Initially, the maximum remains at the same scattering vector but grows in intensity with time. The growth of the intensity as a function of q and time, $I(q,t)$, during this period is effectively described by Cahn–Hilliard theory which predicts that $I(q,t)$ grows exponentially with time, t, and at a rate, $R(q)$, by the proportionality in Eq. (3) [30].

$$I(q,t) \propto \exp[2R(q)t] \tag{3}$$

This exponential growth of $I(q,t)$ is confirmed for both the 40% and 50% samples by semi-logarithmic plots of $\log I$ versus time. As shown in the example for the 40% sample in Fig. 3, this linearity is valid at early illumination times for many different scattering vectors.

According to Cahn–Hilliard theory, the growth rate of the scattered intensity, $R(q)$, is also directly proportional to the composition fluctuations and is defined by Eq. (4) [30].

$$R(q) = D_{app}\, q^2 \left[1 - q^2/\left(2q_m^2\right)\right] \tag{4}$$

The apparent mutual diffusion coefficient, D_{app}, [30–33] in Eq. (4) quantifies the rate of movement of the phase-separating components, q is the scattering vector, and q_m is the wave vector of the scattering maximum. $R(q)$ can thus be determined

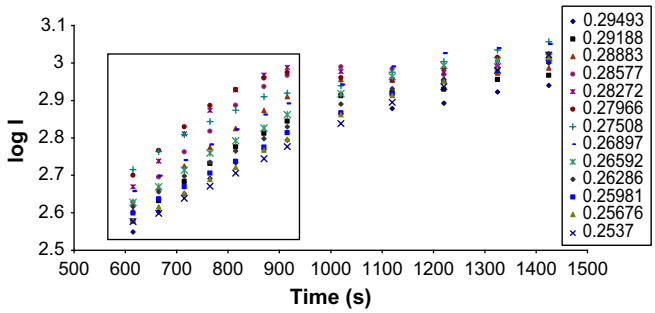

Fig. 3. Semi-logarithmic plot of intensity versus time for different scattering vectors. Slopes of data in boxed section are used to determine the growth rate function, $R(q)$.

from the slope of the linear portion of the semi-logarithmic plots in Fig. 3. A plot of $R(q)/q^2$ versus q^2 thus provides D_{app} from the y-intercept. Such a plot is given in Fig. 4 where the D_{app} for both samples can be found. The 40% sample exhibits a D_{app} of 3×10^{-5} μm^2/s, while the 50% sample has a D_{app} that is nearly an order of magnitude higher, 2×10^{-4} μm^2/s.

The use of this analysis to extract these quantitative parameters is verified by a self-consistent check. The experimentally determined mutual diffusion coefficients are plugged into Eq. (4) to calculate a value of q_m. As q_m is not utilized in the determination of D_{app} from Fig. 3, the equivalence of this calculated q_m and the value found experimentally corroborate the validity of this analysis. The results are shown in Table 1, which shows excellent agreement between the calculated and experimental values, lending further credence to the conclusion that these systems are undergoing early stage spinodal decomposition in this phase separation process. The quantification of the increase in D_{app} with LC content, though not surprising, confirms the change in the mobility of both the matrix material and the LC with increased LC content, a property that contributes to the larger ultimate inter-domain distances of the 50% sample.

As phase separation continues, the interconnected structure of the early stage of SD is expected to break-up into discreet LC domains that are found in the intermediate and late stages

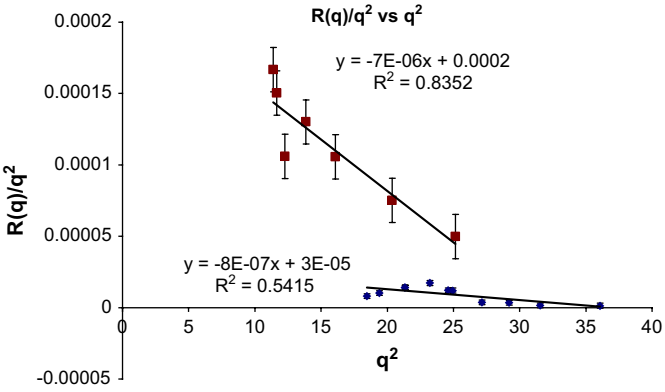

Fig. 4. Growth rate divided by the square of the scattering vector versus the square of the scattering vector, 40% E7 (◆) and 50% E7 (■). y-Intercept gives the apparent mutual diffusion coefficient, D_{app}.

Table 1
Apparent diffusion coefficients, D_{app}, obtained from the analysis of the early stages of spinodal decomposition and maximum scattering vectors, q_m, calculated from D_{app}, compared to experimental results

%E7	D_{app} (μm/s^2)	q_m, calculated (μm^{-1})	q_m, experimental (μm^{-1})
40	3.00E-05	4.08	4.8
50	2.00E-04	3.78	3.4

of SD [30–34]. This transition is seen in the scattering as a shift in the maximum to lower q, an event that appears to occur during the time period of 912–1120 s for the 40% sample and 407–965 s for the 50%. During this transition the growth of the maximum intensity, I_m, as well as the maximum scattering vector, q_m, scales exponentially with time, as described by the theories of Lifshitz and Slyozov [34]. Additionally, the domains should form a self-similar structure during the later stages of SD that grow according to the scaling behavior theorized by Furukawa [34]. However, when the scaling analysis [30] is performed on the scattering maxima for both LC compositions, the results are inconclusive.

In order to determine if either system has actually undergone the transition from early SD to the intermediate/late stages, the LC is removed for the 50% sample, and the resulting film is examined by HRSEM. The HRSEM results, shown in Fig. 5a and b, show the film at lower magnification (Fig. 5a, 10 μm scale bar) and at higher magnification (Fig. 5b, 1 μm scale bar). At low magnification the film appears to lack discreet LC domains, a result confirmed by the micrograph at higher magnification. Instead, the morphology exhibits the presence of an interconnected structure, a structure more in

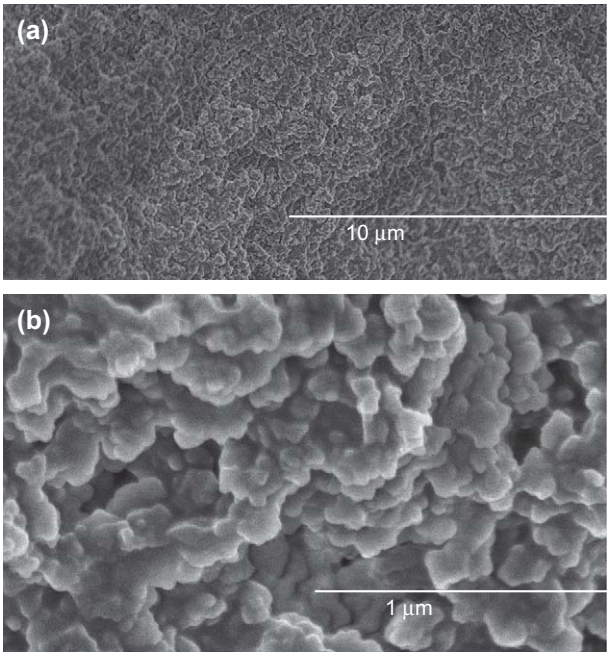

Fig. 5. HRSEM micrographs of films from 50% E7 sample cured at 0.069 mW/cm^2. (a) 10 μm and (b) 1 μm magnification.

keeping with the early stage of SD and is supported by Vaia et al. [18] observations of an interconnected ''Swiss cheese'' morphology in PDLCs cured under much higher cure intensities. This result suggests that, even at low cure intensities, the break-up of the interconnected structure is never reached for these PDLC structures, presumably due to the fast gelation and subsequent vitrification of the polymer matrix [18].

3.2. Higher cure beam intensities

The scattering profiles for both E7 compositions, cured at 0.14 mW/cm^2, can be found in Fig. 6a–d. For the 40% E7 sample, Fig. 6a and b, the earliest recorded time, 14 s, shows the presence of scattering, but no discernable maximum is observed. The total scattering intensity increases between 54 s and 164 s and exhibits a sharp upturn in the forward scattering for lower q-values. The total intensity continues to increase throughout the remainder of the experiment until 618 s where little change of the scattering profiles with time is observed. The 50% E7 samples, Fig. 6c and d, also exhibit scattering at the earliest recorded time, 25 s. For early times, 25–95 s, there appears to be a maximum in the scattering, however, this feature rapidly disappears. As the experiment proceeds to later times, the total intensity increases with a similar upturn in the scattering at low q as the 40% sample.

Scattering profiles for the next higher cure beam intensity, 0.214 mW/cm^2, are shown in Fig. 7a and b. As in the previous experiment, the 40% E7 samples, Fig. 7a, exhibit scattering at the earliest stage of the experiment. In contrast to the 0.14 mW/cm^2 cure intensity, though, the total scattered intensity increases much more rapidly with time. The growth of the scattered intensity continues until the profiles exhibit very little change at 618 s. For the 50% sample, shown in Fig. 7b, the increased cure intensity results in rapid growth of the total scattered intensity, and at 103 s the detector becomes saturated.

The results for the highest of the cure intensities, 0.693 mW/cm^2, used in this study can be found in Fig. 8a

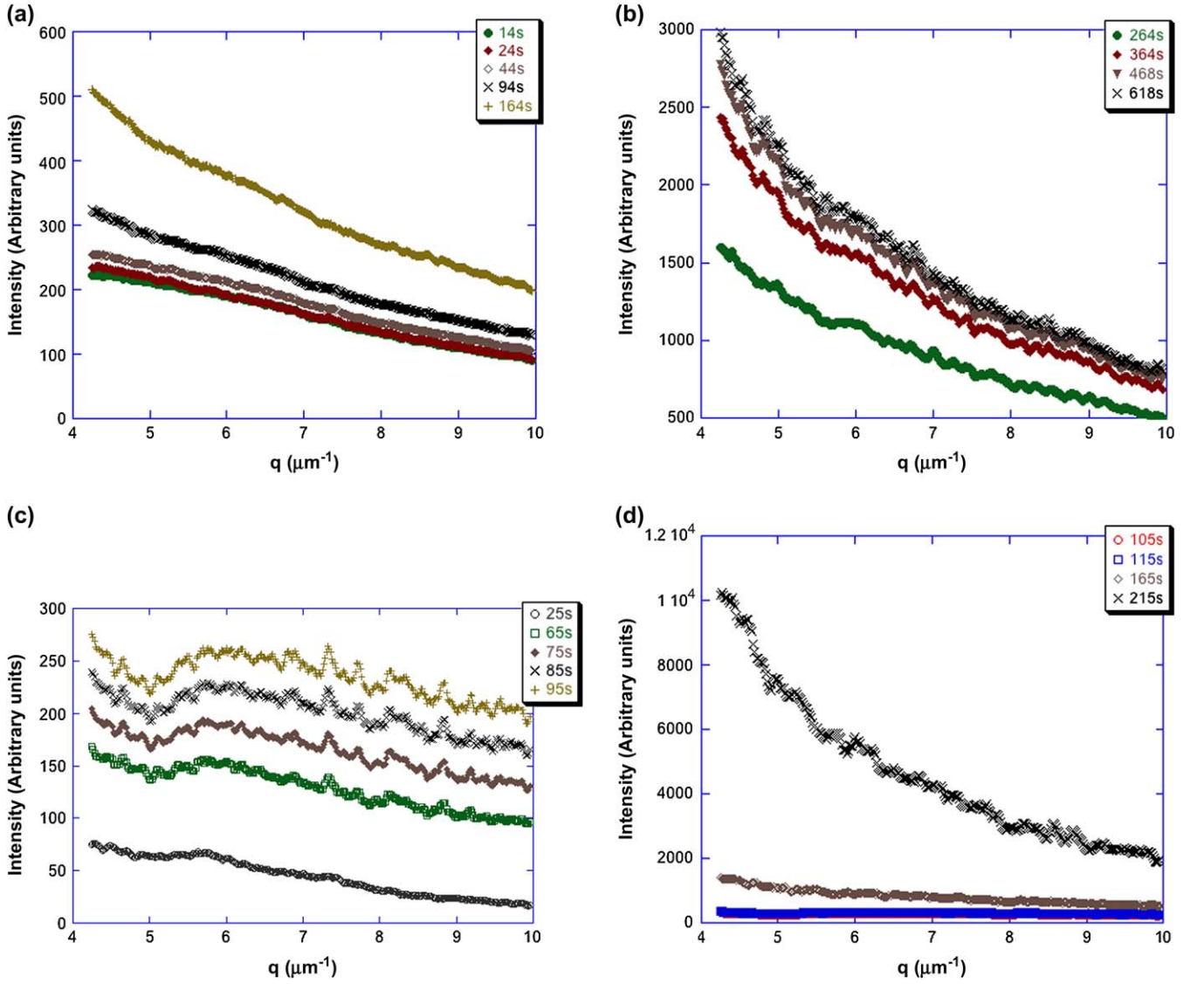

Fig. 6. Scattering profiles for PDLC syrups cured at 0.14 mW/cm^2. (a) 40% E7 14–164 s; (b) 40% E7 264–618 s; (c) 50% E7 25–95 s; (d) 50% E7 105–215 s.

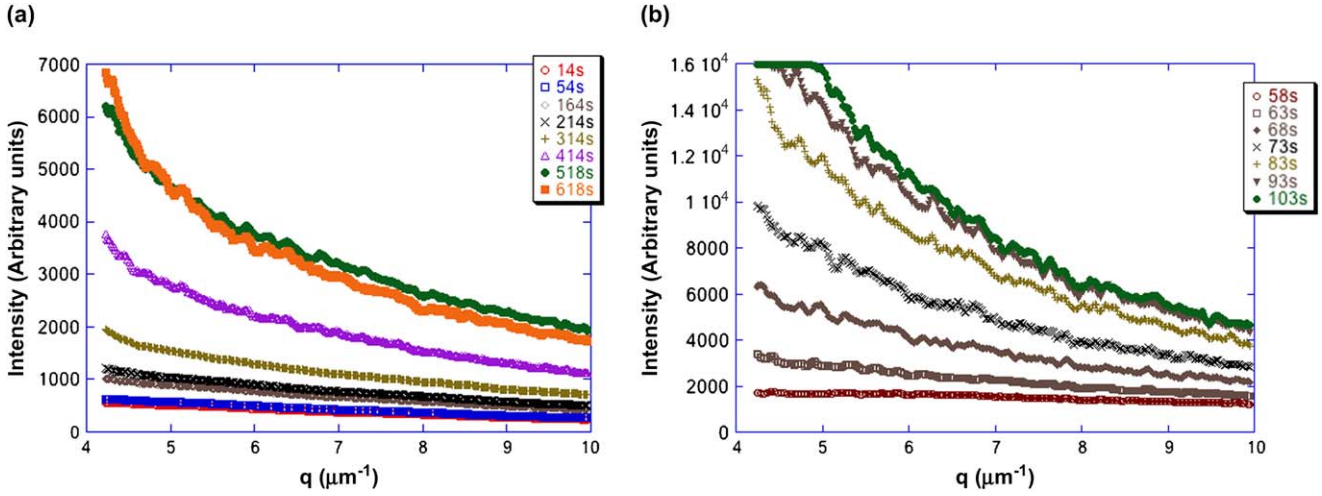

Fig. 7. Scattering profiles for PDLC syrups cured at 0.214 mW/cm^2. (a) 40% E7 14–618 s and (b) 50% E7 58–103 s.

and b. The 40% sample, Fig. 8a, shows much stronger scattering at the outset of the experiment, 11 s. The upturn in scattering at lower q also appears at a much earlier time than in the previous two cure intensities. The total scattered intensity increases with time until 101 s, and afterwards actually decreases until 301 s where there is little further change in the scattering. The 50% sample, Fig. 8b, similar to the 40% sample, exhibits scattering at the earliest stages of the experiment, 15 s, as well as an upturn in the forward scattering at 105 s. The total intensity continues to grow rapidly, but the scattering profile neither shows the decrease in intensity seen in the 40% sample nor reaches the magnitude in intensity observed in the previous 0.214 mW/cm^2 experiment.

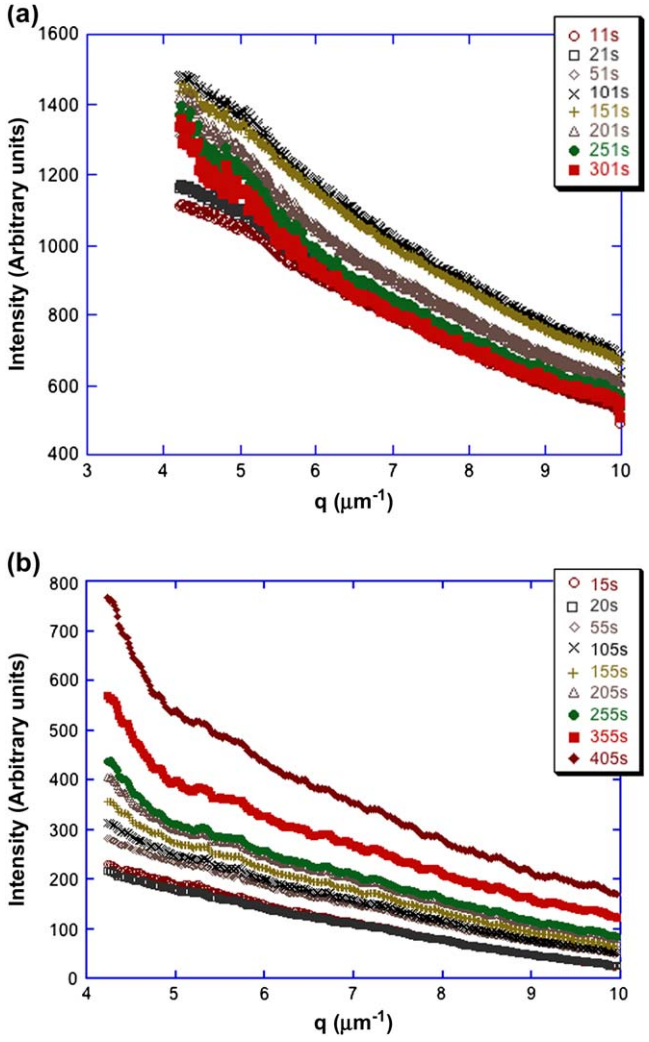

Fig. 8. Scattering profiles for PDLC syrups cured at 0.693 mW/cm^2. (a) 40% E7 11–301 s and (b) 50% E7 15–405 s.

3.3. Analysis of scattering profiles: 0.14–0.693 mW/cm^2

The scattering data from all three-cure intensities possess common features that are independent of LC content or curing conditions. The first feature is the presence of broad scattering with no discernable maximum. This lack of a maximum indicates that, unlike the PDLCs cured at 0.069 mW/cm^2, phase separation via a specific mechanism, i.e. SD or nucleation and growth, cannot be determined from the scattering profiles. Lastly, the scattering profiles show sharp upturns in the forward scattering that may be due to the scattering from phase-separated LC-rich domains.

The presence of broad, featureless scattering profiles implies the formation of a random structure. Since previous studies of the structures of PDLCs that are derived from these syrups show randomly correlated structures, two different models for the scattering of randomly correlated structures can be used to analyze the data. If the PDLC has LC domains that are large enough to appear as a second phase, the Debye–Bueche (DB) [18,35] equation, shown in Eq. (5),

$$I(q) = I(0)/\left(1+\xi^2 q^2\right)^2 \tag{5}$$

describes the scattering behavior. On the other hand, if the LC merely forms fluctuations in the concentration profile, the Ornstein–Zernicke (OZ) equation, [19,36] Eq. (6), is valid.

$$I(q) = I(0)/\left(1+\xi^2 q^2\right) \tag{6}$$

In both equations $I(q)$ is the scattered intensity as a function of scattering vector, q, $I(0)$ is the scattered intensity at $q = 0$, and ξ is the correlation length of the domain or fluctuation.

Although the OZ and DB equations seem similar, the scattering behavior that they describe originates from very different sources. The OZ equation is based on a correlation function that assumes the scattering at low q originates from concentration fluctuations typically found in single-phase systems [36]. The DB equation is also derived from a correlation function, but in this particular model, the low q scattering is due to the presence of inhomogeneities [35] or, in the case of the PDLC, phase-separated LC domains.

In order to determine the proper analysis to use for these PDLC films, the results obtained from each analysis on a single sample are compared to the real-space examination of the same sample by SEM. The analysis that agrees with the real-space image is then utilized. To realize this comparison, TRLS experiments are repeated under similar cure conditions (0.11 and 0.29 mW/cm^2) for one of the samples, the 50% E7 in this case. The scattering profiles for the fully cured films are obtained. Subsequently, the LC is removed from the polymer matrix by immersing the films in methanol and the resultant matrix is examined by HRSEM.

The scattering profiles for the fully cured 50% E7 PDLCs are given in Fig. 9 along with fits of the data to both DB and OZ equations. From the figure it is evident that both equations provide reasonably good fits to the data, however, the two equations yield very different results for both $I(0)$ and ξ. The results from the OZ analysis show that the final value for the correlation length, ξ, is around 12 μm for both cure intensities, while the DB analysis yields 260 nm for 0.11 mW/cm^2 and 230 nm for 0.29 mW/cm^2.

The HRSEM micrographs of the sample for the 0.11 mW/cm^2 experiment can be found in Figs. 10a–d. The first micrograph, Fig. 10a, shows the film with a 10 μm length scale, and Fig. 10b shows the fast Fourier transform (FFT) of this image. The micrograph shows a film with an interconnected [18] morphology that has been shown to be typical in PDLCs formed by floodlit illumination at this LC concentration. The FFT of the micrograph exhibits a completely diffuse pattern that confirms the random distribution needed to apply either OZ or DB [35,36]. The next micrograph, Fig. 10c, shows the same film at 1 μm magnification. The presence of voids in the micrograph indicates that LC domains are being formed during the TRLS experiment. The average size of the voids is determined by taking the plot profile, a typical example of which is shown in Fig. 10d, and measuring the width of the larger voids. The larger voids are only considered as the larger LC domains dominate the scattering measured during the experiment. The average size of the voids is determined by measuring and analyzing the plot profile at various regions of the micrograph and averaging these results, which indicate that the average void size is 145 nm for this sample.

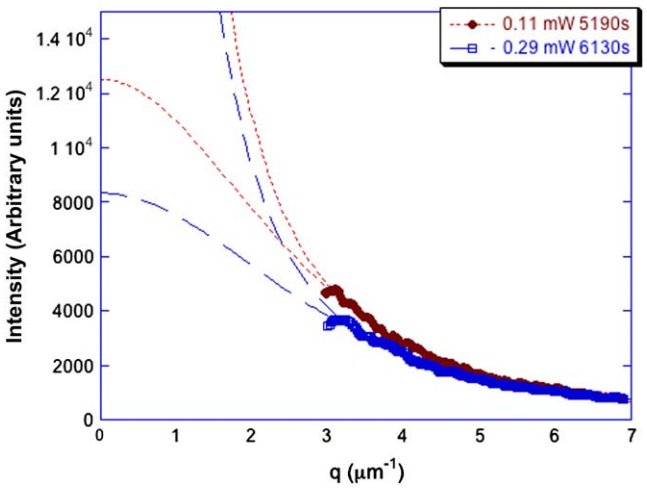

Fig. 9. Scattering profiles for fully cured 50% E7 PDLC films before LC removal.

The film cured at 0.29 mW/cm^2 is analyzed in an identical manner to indicate that the average size of the voids in this sample is approximately 192 nm. Thus, the real-space analysis indicates that the samples are accurately characterized by the use of the DB analysis of the light scattering results.

The results of the DB analyses for both LC compositions at all three-cure intensities are shown in Fig. 11a–c. The $I(0)$ values, which correlate to the number of LC domains present are shown on the left axis, and the correlation length, ξ, of the LC domains are shown on the right axis. It is important to note that the $I(0)$ values are presented in arbitrary units, not absolute units, so factors such as sample transmission and sample thickness can influence its reported value. Thus, comparison of this value between samples must be approached with caution. However, since the samples studied are very similar, this comparison can be utilized in this study. The 0.141 mW/cm^2 cure intensity is shown in Fig. 11a for both LC compositions. The 40% E7 sample exhibits a slow increase in $I(0)$ with time until leveling off at 370 s. The domain size for the 40% sample shows the same growth trend, growing slowly from 70 nm at the start of the experiment and leveling to 170 nm at 370 s. For the 50% E7 sample, $I(0)$ begins to grow slowly, but when the sample has been irradiated for 170 s, $I(0)$ rises steeply throughout the remainder of the experiment until reaching a final value that is nearly three times greater than that of the 40% sample. The domain size for the 50% sample at 25 s is nearly 100 nm and rises quickly to 156 nm at 115 s. Between 115 s and the final time of the experiment, 215 s, the size of the domains decreases to 136 nm before rising again to 198 nm. As the cure intensity is increased to 0.214 mW/cm^2, Fig. 11b, the 40% sample exhibits a smooth, steady increase in $I(0)$ throughout the experiment that reaches a final intensity nearly three times larger than the result in Fig. 11a. The 50% sample also shows a dramatic increase in $I(0)$, attaining a value of almost 40,000 within the first 100 s before the detector becomes saturated. The change in the domain sizes shows similar trends with the 40% sample steadily increasing from 100 to 200 nm and the 50% sample rapidly growing from 20 to 156 nm. For the highest cure intensity, 0.69 mW/cm^2 in Fig. 11c, the DB analysis shows a much different trend from the behavior of the previous two cure intensities. $I(0)$ for 40% shows a rapid increase within the first 100 s

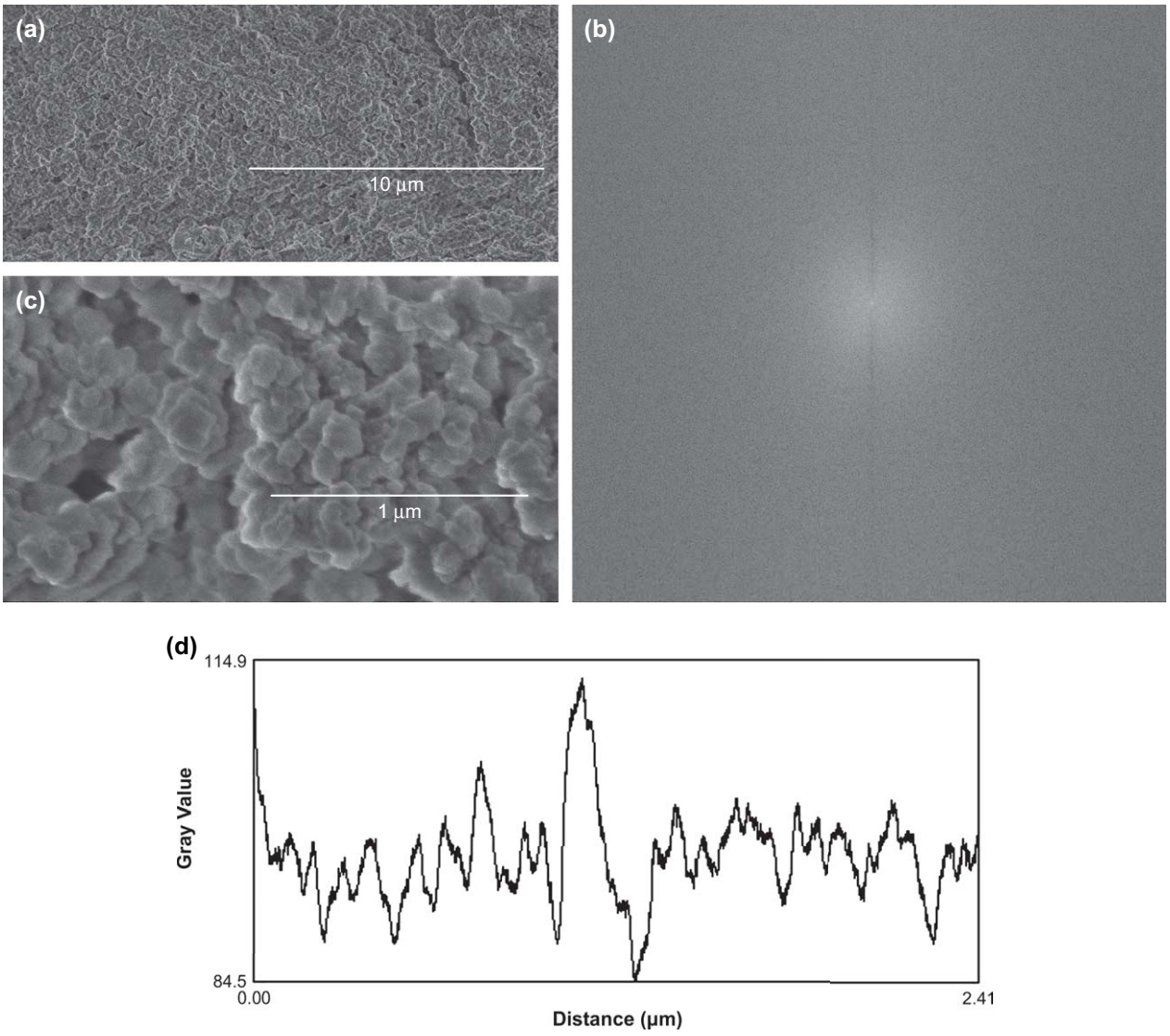

Fig. 10. (a) HRSEM image of PDLC film cured at 0.11 mW/cm^2 (LC has been removed), scale bar 10 μm; (b) FFT of image in (a), indicative of a random network; (c) HRSEM image of PDLC film depicted in Fig. 10a at 1 μm length scale; (d) typical plot profile of image in (c), average size of the voids is approximately 145 nm.

but levels off quickly to values that are much lower than the previous two intensities. As for the 50%, $I(0)$ shows, at first, a very slow increase until 150 s followed by rapid growth, but the final intensity, similar to the 40% sample, never reaches the magnitude of the other experiments. Correlation lengths for the 40% sample start slightly lower, approximately 70 nm, and do not begin to increase until 150 s, approaching a maximum of 120 nm at full cure. ξ for 50% E7 shows domain sizes on the order of 150 nm from the start of the experiment until 150 s when, like the $I(0)$ for this LC composition, the size increases, but instead of continuous growth throughout the remainder of the experiment, ξ levels off to a maximum value of 200 nm.

The results from the DB analysis highlight the consequences of the changing cure intensity on the relative number and size of the LC domains that are formed during PIPS. As the cure intensity is nearly doubled from 0.14 to 0.214 mW/cm^2, the relative number of domains, embodied by $I(0)$, shows dramatic changes for both LC compositions. In the 40% sample the number of LC domains goes from the leveling behavior seen in 11a to the steady increase seen in 11b. Likewise, the 50% sample also shows an increase in the relative number of domains from one cure intensity to the next, but the rate of this increase drastically changes. As a result, the analysis confirms that raising the cure intensity not only creates more LC droplets but also increases the rate of droplet formation. The size of the domains, given by the correlation lengths, also shows marked growth with greater cure intensity, and in the case of the 50% sample, the size of the domains grows over 100 nm in 100 s. A likely explanation for these stems from the increased speed of polymer matrix formation at higher cure beam intensities [18], and since the polymer matrix is being formed at earlier times under the higher cure intensity, the systems are thrust into thermodynamic instability more rapidly. As a result of this faster "quench" [37], the phase separation is not only driven faster but also allows

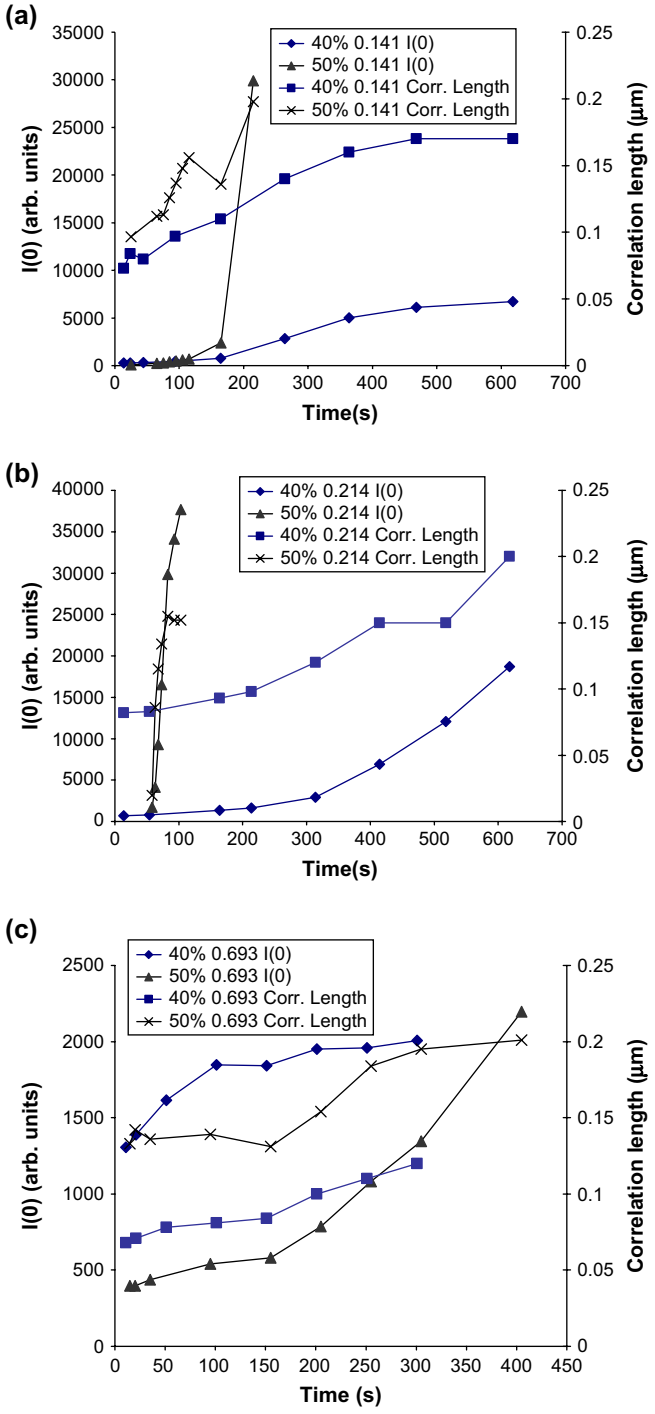

Fig. 11. Debye–Bueche analysis of scattering data, 40% E7 $I(0)$ (◆), 50% E7 $I(0)$ (▲), 40% E7 correlation length (■), 50% E7 correlation length (×). (a) 0.14 mW/cm^2; (b) 0.214 mW/cm^2; (c) 0.693 mW/cm^2.

more time for the LC to separate before the cross-linking/vitrification [18] of the polymer matrix stops phase separation.

Even though the domain formation rate is still quite rapid for the highest beam cure intensity, the cure does not produce as many domains as the other experiments. Similarly, the rate of growth of the LC domains is also affected by the accelerated polymerization at this high beam intensity, as shown by the smaller domain sizes in the 40% sample and the early leveling in the 50% sample. The increased polymerization rate causes a deeper "quench" that speeds up both the formation and the growth of the LC droplets. However, the presence of fewer LC domains as well as the limited domain growth suggests that the cross-linking of the polymer matrix quickly arrests phase separation.

4. Conclusion

The use of time-resolved light scattering to examine the impact of syrup composition and cure beam intensity on the phase separation process in photo-initiated PDLCs provides significant insight into the phase separation process. At the lowest illumination intensity, the early stages of spinodal decomposition are observed and the phase separation process can be evaluated by analyzing the data using the Cahn–Hilliard theory. This analysis shows that the mutual diffusion coefficient in this process is almost an order of magnitude greater in the sample with 50% E7 than the sample with 40% E7. The growth rate of the 40% sample is also about an order of magnitude less than that of the 50% sample, quantifying the extent of change on the rate of phase separation by altering the composition of the initial syrup. At moderate beam cure intensities, the phase decomposition process is more rapid and no evidence of spinodal composition is observed experimentally. However, the resultant structures can be analyzed using the Debye–Bueche model, and this analysis provides a quantification of the change in cure beam intensity and syrup composition on the time evolution of the LC domain size and the number of domains. In this regime, an increase in cure beam intensity results in a system that has faster chain growth, which in turn leads to faster phase separation and larger domains in the ultimate structure. Finally, at even higher cure beam intensities, the results indicate that the chain growth and cross-linking are sufficiently fast to arrest LC domain growth at earlier times, thus resulting in a system with smaller number and size of domains.

Thus, the control of the ultimate domain structure that exists in a PDLC that is created through PIPS via photo-initiated polymerization is quite complex. At low cure beam intensities, an increase in intensity increases the rate of domain formation and the number of domains but if the intensity is increased too much, the rate of polymerization and cross-linking can arrest the phase separation creating a sample that is insufficiently phase separated. As a general rule, the increase in LC content from 40% to 50% results in an increase in the rate of the phase separation process.

References

[1] Collings PJ, Hird M. Introduction to liquid crystals: chemistry and physics. Bristol, PA: Taylor and Francis Ltd; 1997.
[2] Collings PJ, Patel JS. Handbook of liquid crystal research. New York, NY: Oxford University Press; 1997.
[3] Drazic PS. Liquid crystal dispersions. River Edge, NJ: World Scientific Publishing Co.; 1995.
[4] Bunning TJ, Natarajan LV, Tondiglia VP, Sutherland RL. Annual Review of Materials Science 2000;30:83–115.

[5] Mucha M. Progress in Polymer Science 2003;28:837–73.
[6] Jakubiak R, Bunning TJ, Vaia RA, Natarajan LV, Tondiglia VP. Advanced Materials 2003;15(3):241–4.
[7] Ballauff M. Molecular Crystals and Liquid Crystals Letters 1986;4(1): 15–22.
[8] Dorgan JR, Soane DS. Molecular Crystals and Liquid Crystals 1990; 188:129–46.
[9] Benmouna F, Daoudi A, Roussel F, Leclerq L, Busine J, Coqueret X, et al. Macromolecules 2000;33:960.
[10] Kyu T, Shen C, Chiu H-W. Molecular Crystals and Liquid Crystals 1996;287:27.
[11] Ahn W, Kim CY, Kim H, Kim SC. Macromolecules 1992;25:5002–7.
[12] Roussel F, Buisine J, Maschke U, Coqueret X, Benmouna F. Physical Review E Aug. 2000;62(2).
[13] Stroeks A, Nies E. Macromolecules 1990;23:4092.
[14] Gogibus N, Benmouna F, Ewen B, Pakula T, Coqueret X, Benmouna M, et al. Journal of Polymer Science Part B: Polymer Physics 2003; 41:39–43.
[15] Benmouna F, Maschke U, Coqueret X, Benmouna M. Macromolecular Theory and Simulations 2000;9:215–29.
[16] Serbutoviez C, Kloosterboer JG, Boots HMJ, Touwslager FJ. Macromolecules 1996;29:7690–8.
[17] Boots HMJ, Kloosterboer JG, Serbutoviez C, Touwslager FJ. Macromolecules 1996;29:7683–9.
[18] Vaia RA, Tomlin DW, Schulte MD, Bunning TJ. Polymer 2001;42: 1055–65.
[19] Pogue RT, Natarajan LV, Siwecki SA, Tondiglia VP, Sutherland RL, Bunning TJ. Polymer 2000;41:733–41.
[20] Maugey J, Navard P. Polymer 2002;43:6829–37.
[21] Kyu T, Lee JH. Physical Review Letters 1996;76:3746.
[22] Kyu T, Chiu H-W, Lee JH. In: Rosenberg BA, Sigalov GM, editors. Heterophase polymer networks: synthesis, characterization and properties. Gordon and Breach; 2001.
[23] Sato T, Han CC. Journal of Chemical Physics 1988;88(3):2057–65.
[24] Chan PK, Rey AD. Macromolecules 1996;29:8934–41.
[25] Chan PK, Rey AD. Macromolecules 1997;30:2135–43.
[26] Nwabunma D, Kyu T. Macromolecules 1999;32:664–74.
[27] Nwabunma D, Chiu H, Kyu T. Journal of Chemical Physics 2000; 113(15):6429–36.
[28] Kyu T, Chiu H. Polymer 2001;42:9173–85.
[29] Maugey J, Van Nuland T, Navard P. Polymer 2001;42:4353–66.
[30] Matsuyama H, Kudari S, Kiyofuji H, Kitamura Y. Journal of Applied Polymer Science 2000;76:1028–36.
[31] Lauger J, Lay R, Maas S, Gronski W. Macromolecules 1995;28:7010–5.
[32] Fujita K, Kyu T. Macromolecules 1996;29:91–6.
[33] Edel V. Macromolecules 1995;28:6219–28.
[34] Furukawa H. Advances in Physics 1985;34(6):703–50.
[35] Debye P, Bueche AM. Journal of Applied Physics 1949;20:518–25.
[36] Brown W. Light scattering: principles and development. New York, NY: Oxford University Press Inc.; 1996.
[37] Alig I, Rullmann M, Holst M, Xu J. Macromolecular Symposia 2003; 198:245–57.